



**Single-Cell Infrared Vibrational Analysis by Optical Trapping
Mid-Infrared Photothermal Microscopy**

Journal:	<i>Analyst</i>
Manuscript ID	AN-ART-11-2022-001917.R2
Article Type:	Paper
Date Submitted by the Author:	09-Feb-2023
Complete List of Authors:	Kato, Ryo; Tokushima University - Josanjima Campus, Institute of Post-LED Photonics, Yano, Takaaki; Tokushima University - Josanjima Campus, Institute of Post-LED Photonics, Tanaka, Takuo; RIKEN, Metamaterials lab.

Single-Cell Infrared Vibrational Analysis by Optical Trapping Mid-Infrared Photothermal Microscopy

Ryo Kato, Taka-aki Yano, * and Takuo Tanaka*

¹ Institute of Post-LED Photonics, Tokushima University, 2-1 Minamijosanjima-cho, Tokushima, Tokushima 770-0856

² Innovative Photon Manipulation Research Team, RIKEN Center for Advanced Photonics, Wako, Saitama 351-0198, Japan

³ Metamaterials Laboratory, RIKEN Cluster for Pioneering Research, Wako, Saitama 351-0198, Japan

* Corresponding authors: yano.takaaki@tokushima-u.ac.jp
t-tanaka@riken.jp

Abstract

Single-cell analysis by means of vibrational spectroscopy combined with optical trapping is a reliable platform for unveiling cell-to-cell heterogeneities in vast populations. Although infrared (IR) vibrational spectroscopy provides rich molecular fingerprint information on biological samples in a label-free manner, its applications with optical trapping has never been achieved due to weak gradient forces generated by the diffraction-limited focused IR beam and strong background of water absorption. Herein, we present single-cell IR vibrational analysis that incorporates mid-infrared photothermal (MIP) microscopy with optical trapping. Optically trapped single polymer particles and red blood cells (RBCs) in blood could be chemically identified owing to their IR vibrational fingerprints. This single-cell IR vibrational analysis further allowed us to probe the chemical heterogeneities of RBCs originating from the variation in the intracellular characteristics. Our demonstration paves the way for the IR vibrational analysis of single cells and chemical characterization in various fields.

Introduction

Single-cell analysis is a powerful tool for understanding the fundamental behaviors of biological systems and for developing new therapeutic applications for autoimmune disorders and circulating tumor cells.¹⁻³ Hence, there has been an increase in the demand for advanced technologies for single-cell analysis based on the morphology or chemical compositions of cells, to reveal cell-to-cell heterogeneities in vast populations that can be lost in conventional bulk experiments. Raman spectroscopy and infrared (IR) absorption spectroscopy are promising for fetching chemical information on molecules in a label-free manner. They are widely used not only in the studies of cells and tissues,^{4,5} but also for the chemical characterization of carbon and semiconductor materials⁶ and polymers.⁷ Moreover, the combination of Raman spectroscopy with optical trapping has attracted much attention for single-cell analysis since it allows simultaneous trapping/manipulation and stable Raman analysis of single cells, which invariably move due to their Brownian motion in an aqueous solution.⁸ Optical trapping has proven its capability of grasping and manipulating micrometer-scale objects. In particular, biological studies have been put forward by optical trapping, where cell sorting⁹ and single-cell analysis¹⁰ were achieved. In optical trapping, a visible or near-IR laser beam is tightly focused to create gradient forces. A tiny object located near the focus spot experiences the gradient forces and is stabilized within the focus spot. The combination of optical trapping with Raman spectroscopy has been explored by many groups.¹¹⁻¹³ In contrast, although the IR absorption cross-section of primary biomolecules is much higher than that obtained by Raman scattering, the IR vibrational analysis of optically trapped single cells in liquid has never been achieved. This is because conventional Fourier transform infrared (FTIR) spectroscopy utilizes a broadband IR light source with low power density, thereby the gradient forces induced by the diffraction-limited focused IR beam are not sufficient to immobilize a single object in a liquid. Since the IR absorption of cells reflects the vibrational

1
2
3
4
5
6 modes of primary biological molecules, such as amide I and amide II bands from proteins, and
7
8 COO⁻ stretching mode of carbohydrates, fatty acids, and amino acid proteins, the IR vibrational
9
10 analysis of biological samples has been useful for many applications,¹⁴ including discrimination
11
12 of protein secondary conformation¹⁵ and monitoring the uptake and metabolism of isotopically
13
14 labeled fatty acids.¹⁶ Thus, there is a high demand for the integration of IR vibrational
15
16 spectroscopy and optical trapping to realize the single-cell IR vibrational analysis.
17
18

19
20 Recently, a novel IR spectroscopic technique called as mid-infrared photothermal (MIP)
21
22 microscopy was developed.¹⁷⁻¹⁹ MIP microscopy leverages both, IR and visible laser beams, to
23
24 measure IR absorption of molecules by probing the change in the refractive index of the sample
25
26 on account of a local temperature change upon absorption of the pulsed IR beam. Importantly, the
27
28 tightly focused visible probe beam can also be utilized as a trapping laser. Moreover, MIP
29
30 microscopy also helps in overcoming the other drawback in conventional FTIR spectroscopy
31
32 faced due to the water absorption background, owing to its configuration of signal transduction;
33
34 this has demonstrated in the chemical characterization of cells in a liquid^{20,21} and single-cell
35
36 analysis of bacterial samples.²²
37
38

39
40 Herein, we present an IR vibrational analysis of optically trapped individual polymer particles
41
42 and red blood cells (RBCs) in a liquid using MIP microscopy. Single-cell IR analysis of optically
43
44 trapped samples allowed us to not only chemically identify RBCs in blood, where a number of
45
46 blood components coexist, but also to probe chemical heterogeneities in individual RBCs. Our
47
48 study emphasizes the benefits of this technique for versatile studies, including those on single-
49
50 cell chemical analysis and cell sorting.
51
52
53
54
55
56
57
58
59
60

Experimental Section

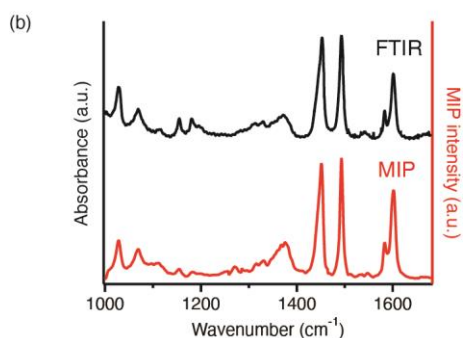
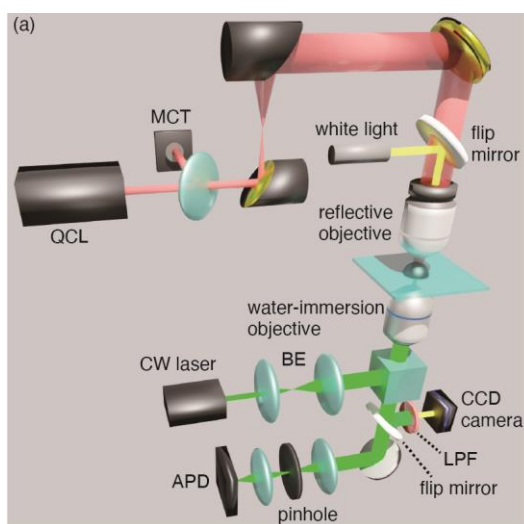
Sample preparation

One microliter of polystyrene beads (PS beads, Micromod Partikeltechnologie) with a diameter of 3.5 μm were diluted in 15 μL of D_2O -PBS. The sample solution was then sonicated for 1 min to disperse beads and subsequently dropped on a glass cover slip sandwiched by a CaF_2 cover slip. The blood samples used in all experiments were appropriately treated under ethical regulations of Tokushima University and were purchased from COSMO BIO Co., LTD., (EDTA-2K, certification number: 1072765) with an informed consent from a health volunteer. The 50 μL of the blood solution were casted on a cover slip without any dilution and the sample was sandwiched with a CaF_2 substrate.

Optical setup of MIP microscopy

Figure 1(a) shows the optical setup for MIP spectroscopy with optical trapping. For the MIP measurements, a tunable quantum cascade laser (QCL, Daylight Solutions, MIRcat-QT-2100) with a wavenumber range of 1000–1690 cm^{-1} was used as a pulsed mid-IR (MIR) pump light source. The QCL was operated at a repetition rate of 80 kHz with a pulse width of 500 ns. The spectral resolution of MIP spectra is determined by the spectral data point spacing namely the step size for sweeping the wavelength of QCL, which we set to 1 or 3 cm^{-1} depending on measurements because the wavelength accuracy of our QCL is less than 1 cm^{-1} and the spectral line width of IR light from the QCL is 1 cm^{-1} . The dwell time for each wavenumber to acquire reasonable photothermal responses was 200 ms, thereby it takes 50 s to record an MIP spectrum with the spectral data point spacing to 3 cm^{-1} in the entire fingerprint region. The power of the pulsed IR beam was set to 1 mW for all measurements. A Ge window (10 % reflection) was used to guide the residual IR beam to a mercury cadmium telluride (MCT) detector (Thorlabs,

1
2
3
4
5
6 PDAVJ10) to monitor the power spectrum of the QCL. The diameter of the incident MIR beam
7
8 was expanded by three times using two parabolic gold mirrors. The MIR beam was focused on
9
10 the sample using a reflective objective (Thorlabs, 40 \times /NA 0.5). A continuous-wave (CW) visible
11
12 laser with a wavelength of 532 nm (ELFORLIGHT, G4-200) was used for the optical trapping
13
14 and MIP measurements of polymer particles and the one with a wavelength of 660 nm (Laser
15
16 Quantum, gem660) was used for measurements of RBCs. The diameter of the visible beam was
17
18 expanded using a beam expander, and the beam was reflected by a beam splitter
19
20 (reflection:transmission = 10:90). We used a counter-propagating visible beam focused by a high-
21
22
23



53 Figure 1 (a) Schematic of the MIP microscopy setup. QCL: quantum cascade laser, MCT:
54 mercury cadmium telluride detector, BE: beam expander, LPF: long-pass filter, APD:
55 avalanche photodiode. (b) Comparison of FTIR and MIP spectra of PS beads.
56
57
58
59
60

1
2
3
4
5
6 NA water-immersion objective (Olympus, 60×/NA 1.2), which contributed to robust optical
7
8 trapping as well as a high detection sensitivity of the optical signal. The visible output signal was
9
10 collected using the same objective. After passing through a pinhole with a diameter of 50 μm , the
11
12 output signal was detected using an avalanche photodetector (Thorlabs, APD430A2/M). The
13
14 detected signal was guided to a lock-in amplifier (NF Electronic Instruments, LI5660) for the
15
16 phase-sensitive detection of the MIP signal, which was modulated by the QCL repetition rate. To
17
18 monitor the optical trapping, white light was guided to the sample from the top, and bright-field
19
20 images were obtained using a CCD camera. A long-pass filter was used to block the visible CW
21
22 laser. For control measurement, chemical analysis of samples was performed using FTIR (Fourier
23
24 transform infrared) spectrometer in transmission mode (JASCO Corporation, FTIR-6800). A
25
26 spectral range in FTIR measurements was set from 1000 to 3000 cm^{-1} with a spectral resolution
27
28 of 2 cm^{-1} . All samples for FTIR measurements were dry-casted on CaF_2 cover slips. The spectral
29
30 fidelity of the MIP microscope was confirmed by acquiring the MIP and FTIR spectra of PS beads
31
32 with a diameter of 3.5 μm . Figure 1(b) shows the MIP and FTIR spectra of the PS beads on a
33
34 CaF_2 coverslip. There is good consistency on IR absorption peaks detected between the MIP
35
36 spectrum and the FTIR spectrum, such as the peak position and the peak intensity ratio in the mid-
37
38 IR fingerprint region. It should be noted that all MIP spectra in the present study were normalized
39
40 by IR power spectrum detected by MCT detector taking the variation of the size of the diffraction
41
42 limited IR focus spot into account since the variation of IR wavelength affects the power density
43
44 of IR laser at the focus spot.
45
46
47
48
49
50
51
52
53
54
55
56
57
58
59
60

Results and Discussion

We demonstrated the simultaneous MIP spectroscopic measurements and optical trapping of single PS beads. Figures 2(a)–(c) show the snapshots of an optically trapped PS bead. The power of the visible probe beam with a wavelength of 532 nm was set at 4 mW. The position of the tightly focused laser spot is indicated by the green dotted circle in Figure 2(a). When the PS bead approached the focus spot, it was trapped (Figure 2(a)). The PS bead was manipulated in the transverse direction by moving the sample stage in the x-y axis (Figures 2(b) and 2(c)). The MIP spectrum of the optically trapped PS bead is shown in Figure 2(d), where the primary IR vibrational modes of polystyrene appear at 1450 cm^{-1} , 1494 cm^{-1} , and 1600 cm^{-1} originating from the CH_2 bending mode and aromatic stretching vibrations were clearly observed. Relatively weak signal intensity in the low wavenumber region was ascribed to the low signal to noise (S/N) ratio owing to absorption of D_2O . The results prove that our MIP system is capable of capturing single objects and performing the in-situ IR vibrational analysis of the objects in a liquid. The entire MIP measurement process along with optical trapping of the PS bead is shown in Supporting Information Movie S1. The stability of MIP signal during optical trapping is important particularly when dynamic biological processes and phenomena associated with tiny change of

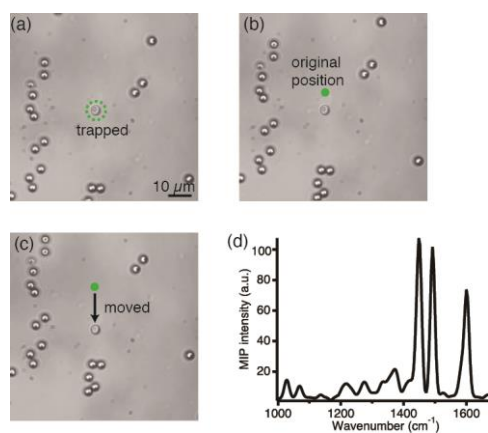
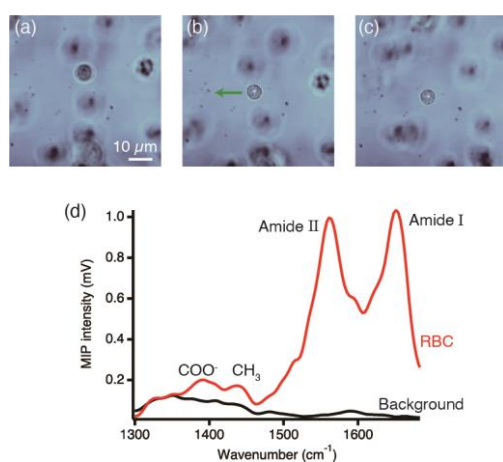


Figure 2 (a)-(c) Snapshots of an optically trapped and manipulated single PS bead. (d) MIP spectrum of the optically trapped single PS bead.

1
2
3
4
5
6 chemical structure of molecules are investigated in a reproducible manner. We further investigated
7
8 the time-dependent MIP signal intensity of an optically trapped PS bead to evaluate the stability
9
10 of the MIP measurement with optical trapping as shown in Figure S1 in Supporting Information
11
12 and confirmed that stable MIP measurement can be performed.

13
14
15 Next, we employed MIP microscopy for single-cell analysis under liquid conditions. We
16
17 demonstrated the IR vibrational analysis of optically trapped single RBCs in blood, where a
18
19 variety of blood components, including RBCs, plaque, leukocytes, and impurities, coexist. RBCs
20
21 are the most abundant cell type in the human blood. Since several critical diseases, such as
22
23 autoimmune disorders, are associated with heterogeneities of RBCs,²³ there has extensive focus
24
25 on fingerprinting the IR vibrational modes of optically trapped RBCs at the single-cell level.
26
27 Figures 3(a)-(c) show snapshots of the optical-trapping MIP measurements of a single RBC. First,
28
29 a single RBC shown in Figure 3(a), was optically and selectively trapped from different blood
30
31 components. The trapped RBC is subsequently manipulated in the transverse direction by moving
32
33 the microscope stage. The RBC is placed where other blood components are absent, as shown in
34
35 Figure 3(c). In the MIP measurements, the power of the visible probe beam with a wavelength of
36
37 660 nm was kept at less than 4 mW, which is a lower laser power compared to that employed in
38
39 previous studies, in order to prevent possible photodamage of the RBCs during MIP
40
41 measurement.^{24,25} It should be noted that we confirmed that the visible probe beam did not give
42
43 notable photodamage to RBC samples during measurements by continuously acquiring three MIP
44
45 spectra of the same RBC, as shown in Figure S2 in Supporting Information. Figure 3(d) shows
46
47 the MIP spectrum of a single RBC together with the background spectrum of blood solution, in
48
49 which substances in plasma including anticaking agent is more likely detected. It should be noted
50
51 that the effect of IR absorption of water could be reduced in our MIP measurement since the
52
53 visible probe signal, which is mostly scattered and reflected light from substances, such as
54
55
56
57
58
59
60

1
2
3
4
5
6 molecules and a substrate, was dominantly detected and used to extract photothermal response of
7
8 IR absorption. The MIP spectrum shows strong characteristic peaks of proteins originating from
9
10 the amide I band at 1660 cm^{-1} and the amide II band at 1560 cm^{-1} , and relatively weak bands: the
11
12 CH_3 stretching mode of various molecular components in cells around 1440 cm^{-1} , and COO^-
13
14 stretching mode of fatty acids and amino acid side chains around 1390 cm^{-1} . It is well known that
15
16 the peak position of the amide I band is sensitive to the secondary conformation of proteins.
17
18 Proteins that possess α -helices in secondary structures exhibit the amide I band around 1640 - 1660
19
20 cm^{-1} , while for β -sheets in secondary structures, the amide I band appears around 1620 - 1640 cm^{-1} .
21
22 ^{1,26} The amide I band at 1660 cm^{-1} in the MIP spectrum of the single RBC indicates the dominant
23
24 presence of the α -helical structure in the RBC. This agrees with the fact that the major constituent
25
26 of RBCs ($\sim 80\%$) is hemoglobin, which is a protein mostly composed of α -helical structures.⁸ We
27
28 would like to mention that further chemical analysis based on other IR absorption bands in the
29
30 low wavenumber region, such as 1050 cm^{-1} of PO_2^- derived from phospholipids would be
31
32 insightful for biological studies while the present study focuses on the higher wavenumber region
33
34 (1300 - 1700 cm^{-1}) since the S/N ratio was not good enough in the lower wavenumber region.
35
36
37
38
39
40



55
56 Figure 3 (a)-(c) Snapshots of an optically trapped and manipulated single RBCs. (d) MIP
57 spectrum of the optically trapped RBC and background spectrum of buffer solution.
58
59
60

1
2
3
4
5
6 We extended the optical trapping MIP microscopy to a single-cell IR vibrational analysis of
7
8 RBCs in human blood. Figure 4(a) displays the MIP spectra of different optically trapped single
9
10 RBCs. Typical single RBCs measured for the MIP spectrum 6 and the MIP spectra 8 were shown
11
12 in Figures 4(b) and 4(c), respectively. Indeed, it is hard to chemically identify the differences
13
14 between the two RBCs only by the optical images. In most MIP spectra, the similar characteristic
15
16 peaks of RBCs can be seen. However, there are detectable differences of spectral characteristics
17
18 between them at the single-cell level. For example, the relative peak intensity of the amide II band,
19
20 CH_3 stretching mode, and COO^- stretching mode against amide I band varied among MIP spectra.
21
22 The intensity ratio between Amide I band and Amide II band (red dots), CH_3 stretching mode
23
24 (green dots), and COO^- stretching mode (blue dots) was given out respectively in Figure 4(d).
25
26 Interestingly, the tendency of the intensity ratio for three peaks are somehow connected except
27
28 RBC 5 and 7. This indicates that the variation of intracellular components other than hemoglobin,
29
30 such as lipids and proteins was detected by MIP measurement as previously studied by FTIR
31
32 measurement of biological samples.²⁷ The intensity ratio of COO^- and CH_3 was relatively low in
33
34 RBC 5 and 7, which could be attributed to a relatively high content of proteins in the detection
35
36 volume. Since the RBCs were optically trapped by the tightly focused visible beam, the
37
38 orientation of all RBCs was similar, which allows one to exclude the possibility of the orientation
39
40 dependence of MIP spectra. Since the focused spot size of the visible probe beam is about 300
41
42 nm in our present setup, the measurement location is considered to be the center of cells within
43
44 the deviation of less than 150 nm. According to previous work, MIP microscopy with the spatial
45
46 resolution of the several hundred nanometer allows one to reveal chemical heterogeneities inside
47
48 cells.²⁸ However, such subcellular spectral variations attributed to measurement locations were
49
50 not seen in our MIP spectra of an optically trapped single RBC continuously recorded 3 times,
51
52 exhibited in Figure S2 in Supporting Information. If the subcellular spectral variation depending
53
54
55
56
57
58
59
60

on measurements is seen in our MIP measurement, the three MIP spectra should be varied even though the analyzed cell is same. Hence, we believed that the subcellular spectral variation in the same sample should not be reflected in our MIP measurement. Hence, the possible reason for spectral variations is that our MIP spectra of single RBCs reflects cell-to-cell chemical heterogeneities. The variation of the intensity ratio between the amide I band and other bands in MIP spectra indicates relative contents of intracellular compositions,²⁹ denaturation of proteins, or existence of extracellular vesicles and other blood components in the detection volume. We would like to point out that such variation of IR absorption bands of RBCs cannot be probed using conventional FTIR measurement because it detects IR characteristic bands of assembled RBCs, so that single cellular character is buried as shown in FTIR data of RBCs casted on a CaF₂ cover slip (Figure S3 in Supporting Information). It would be instructive to see the differences of spectral features among other blood components, such as lymphocytes^{30,31} and platelets³² in

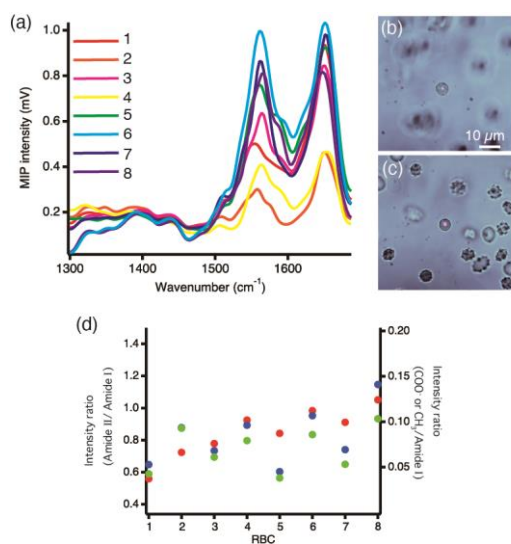


Figure 4 (a) MIP spectra of 8 different RBCs in blood. (b), (c) Optical images of typical RBCs measured for spectrum 6 and spectrum 8 in Figure 4(a). (d) Intercellular comparison of intensity ratios of different IR absorption bands against the Amide I band in spectra of 8 different RBC. Red, green, and blue dots represent the intensity ratio between Amide I band and Amide II, CH₃, and COO⁻, respectively.

1
2
3
4
5
6 plasma as previous work demonstrated FTIR analysis of blood components. For example,
7
8 lymphocytes have similar IR vibrational characteristic, but detectable differences of Amide band
9
10 ratio while platelets obviously have weak Amide II and Amide III band intensity. Optical trapping
11
12 MIP microscopy can collect and analyze IR vibrational signatures of single blood components in
13
14 solution, thereby it allows us to reveal interest in biochemical research, such as the effect of
15
16 plasma on the IR spectra of blood components. Although the further investigation should be
17
18 needed to identify the origin of cell-to-cell variation associated with chemical constitutes, at least
19
20 it was demonstrated that our optical trapping MIP microscopy provides platform for chemical
21
22 characterization of single particles and cells in liquid based on IR absorption and could be
23
24 employed for various biochemical applications, such as cell sorting and bacterial identification.
25
26
27

28 We would like to mention here that the multimodal detection of complementary vibrational
29
30 signals of molecules, such as Raman scattering signals, would also provide more detailed
31
32 chemical information of the sample and increase the molecular specificity, leading to a higher
33
34 accuracy of cell classification.¹⁹ In the sense of the maximum size of cells that can be optically
35
36 trapped, we can reasonably trap objects around 10 μm in size in our current setup, which is
37
38 comparable to ordinary optical trapping spectroscopic systems.¹⁰ Although the use of the higher
39
40 laser power enables to trap bigger objects, there is a trade-off relation between the trapping force
41
42 and photodamage to the sample.
43
44
45

46 **Conclusion**

47
48 We demonstrated the integration of MIP microscopy and optical trapping for the IR vibrational
49
50 analysis of single cells in a liquid. Using MIP microscopy, in which a tightly focused visible beam
51
52 is used to probe the IR absorption of the samples, we performed the in-situ IR vibrational
53
54 spectroscopy of optically trapped single polymer particles and cells. The optical trapping MIP
55
56 microscopy achieved single-cell IR vibrational analysis, which allowed us to study single RBCs
57
58
59
60

1
2
3
4
5
6 in human blood and probe the differences in chemical signatures of single RBCs suggesting the
7
8 slight variation in the chemical compositions of RBCs. IR vibrational spectroscopy using MIP
9
10 microscopy with optical trapping is highly promising for the chemical analysis of biological
11
12 samples. For example, the high spatial resolution of MIP microscopy and optical trapping enables
13
14 both, the trapping and detection of not only single cells but also organelles within cells. This
15
16 technique is highly compatible with flow cytometry and microfluidic devices, which realize
17
18 robust and reliable cell sorting systems.³³ The optical-trapping MIP microscopy technique
19
20 developed herein would open new routes for numerous biological studies, such as the non-
21
22 invasive chemical identification of various types of single cells, discovery of cell-to-cell
23
24 heterogeneities, biochemical interactions between cells, and single-cell sequencing with chemical
25
26 signatures. This technique can also accelerate the use of MIP microscopy for chemical
27
28 characterization in a wide range of fields, such as catalysis, polymer science, and nanotechnology.
29
30

31 32 **Supporting Information**

33
34 Normalized time-dependent MIP signal intensity of an optically trapped single PS bead, MIP
35
36 spectra of an optically trapped single RBC continuously recorded 3 times, comparison of the FTIR
37
38 spectrum of ensemble of RBCs and the MIP spectrum of single RBCs, and optical trapping and
39
40 MIP spectroscopy of a single PS bead (MP4)
41
42

43 **Author contributions**

44
45 All authors equally contributed to the present study for formal analysis, funding, and manuscript
46
47 writing. R.K. conceived the methodology and performed experiments.
48
49

50 **Conflicts of interest**

51
52 There are no conflicts to declare.
53

54 **Acknowledgements**

55
56 This research was supported in part by Nakatani foundation, JSPS KAKENHI grant no. JP21K20503
57
58 (R.K.), JST ACT-X grant no. JPMJAX21B4 (R.K.), JST FOREST grant no. JPMJFR202I (T.Y.), JST
59
60 CREST grant no. JPMJCR1904 (T.T.), and COI-NEXT grant no. JPMJPF2011 (R.K. and T.Y.) from

1
2
3
4
5
6 the Japan Science and Technology Agency, JST. We also acknowledge the financial support from the
7 project on the Promotion of Regional Industries and Universities by the Cabinet Office, and the Plan
8 for Industry Promotion and Young People's Job Creation by the Creation and Application of Next-
9 Generation Photonics by Tokushima Prefecture.
10
11

12 **ORCID ID**

13
14 Ryo Kato: <https://orcid.org/0000-0002-9134-1382>

15
16 Taka-aki Yano: <https://orcid.org/0000-0003-0063-6407>

17
18 Takuo Tanaka: <https://orcid.org/0000-0001-5714-5401>
19
20

21 **References**

- 22
23 1 J. R. Heath, A. Ribas and P. S. Mischel, *Nat. Rev. Drug Discov.*, 2016, **15**, 204–216.
24
25 2 D. Lin, L. Shen, M. Luo, K. Zhang, J. Li, Q. Yang, F. Zhu, D. Zhou, S. Zheng, Y. Chen
26 and J. Zhou, *Signal Transduct. Target. Ther.*, 2021, **6**, 404.
27
28 3 J. Saito, X. Deng and A. Okamoto, *Anal. Chem.*, 2020, **92**, 15616–15623.
29
30 4 A. Sakane, T. aki Yano, T. Uchihashi, K. Horikawa, Y. Hara, I. Imoto, S. Kurisu, H.
31 Yamada, K. Takei and T. Sasaki, *Commun. Biol.*, 2021, **4**, 1–16.
32
33 5 C.-C. Hsu, J. Xu, B. Brinkhof, H. Wang, Z. Cui, W. E. Huang and H. Ye, *Proc. Natl.*
34 *Acad. Sci.*, 2020, **117**, 18412–18423.
35
36 6 T. A. Yano, K. Yoshida, Y. Hayamizu, T. Hayashi, F. Ohuchi and M. Hara, *2D Mater.*,
37 2015, **2**, 035004.
38
39 7 W. Wang, F. Shao, M. Kröger, R. Zenobi and A. D. Schlüter, *J. Am. Chem. Soc.*, 2019,
40 **141**, 9867–9871.
41
42 8 C. Ghanashyam, S. Shetty, S. Bharati, S. Chidangil and A. Bankapur, *Anal. Chem.*,
43 2021, **93**, 5484–5493.
44
45 9 X. Wang, S. Chen, M. Kong, Z. Wang, K. D. Costa, R. A. Li and D. Sun, *Lab Chip*,
46 2011, **11**, 3656–3662.
47
48
49
50
51
52
53
54
55
56
57
58
59
60

- 1
2
3
4
5
6 10 T. Fang, W. Shang, C. Liu, J. Xu, D. Zhao, Y. Liu and A. Ye, *Anal. Chem.*, 2019, **91**,
7
8 9932–9939.
9
10
11 11 C. Xie, J. Mace, M. A. Dinno, Y. Q. Li, W. Tang, R. J. Newton and P. J. Gemperline,
12
13 *Anal. Chem.*, 2005, **77**, 4390–4397.
14
15 12 P. Adgett, A. M. I. R. M. G. Haemmaghami and I. O. A. N. N. Otingher, *Opt. Express*,
16
17 2018, **26**, 25211–25225.
18
19 13 M. Wu, D. Ling, L. Ling, W. Li and Y. Li, *Sci. Rep.*, 2017, **7**, 42930.
20
21
22 14 T. Tanaka, T. Yano and R. Kato, *Nanophotonics*, 2022, **11**, 2541–2561.
23
24 15 A. Troullier, D. Reinstädler, Y. Dupont, D. Naumann and V. Forge, *Nat. Struct. Biol.*,
25
26 2000, **7**, 78–86.
27
28 16 L. Shi, X. Liu, L. Shi, H. T. Stinson, J. Rowlette, L. J. Kahl, C. R. Evans, C. Zheng, L.
29
30 E. P. Dietrich and W. Min, *Nat. Methods*, 2020, **17**, 844–851.
31
32
33 17 K. Aleshire, I. M. Pavlovetc, R. Collette, X. T. Kong, P. D. Rack, S. Zhang, D. J.
34
35 Masiello, J. P. Camden, G. V. Hartland and M. Kuno, *Proc. Natl. Acad. Sci. U. S. A.*,
36
37 2020, **117**, 2288–2293.
38
39 18 Y. Bai, D. Zhang, L. Lan, Y. Huang, K. Maize, A. Shakouri and J. X. Cheng, *Sci. Adv.*, ,
40
41 DOI:10.1126/sciadv.aav7127.
42
43
44 19 R. Kato, T. Yano and T. Tanaka, *Vib. Spectrosc.*, 2022, **118**, 103333.
45
46 20 A. Spadea, J. Denbigh, M. J. Lawrence, M. Kansiz and P. Gardner, *Anal. Chem.*, 2021,
47
48 **93**, 3938–3950.
49
50
51 21 J. Yin, L. Lan, Y. Zhang, H. Ni, Y. Tan, M. Zhang, Y. Bai and J. X. Cheng, *Nat.*
52
53 *Commun.*, 2021, **12**, 1–11.
54
55 22 J. Xu, X. Li, Z. Guo, W. E. Huang and J. X. Cheng, *Anal. Chem.*, 2020, **92**, 14459–
56
57 14465.
58
59
60

- 1
2
3
4
5
6 23 H. Li, L. Lu, X. Li, P. A. Buffet, M. Dao, G. E. Karniadakis and S. Suresh, *Proc. Natl.*
7
8 *Acad. Sci.*, 2018, **115**, 9574–9579.
9
- 10 24 S. Ahlawat, N. Kumar, R. Dasgupta, R. Shanker Verma, A. Uppal and P. K. Gupta,
11
12 *Appl. Phys. Lett.*, 2013, **103**, 183704.
13
- 14 25 M. A. S. De Oliveira, Z. J. Smith, F. Knorr, R. E. De Araujo and S. Wachsmann-Hogiu,
15
16 *Appl. Phys. Lett.*, , DOI:10.1063/1.4868253.
17
- 18 26 O. Klementieva, C. Sandt, I. Martinsson, M. Kansiz, G. K. Gouras and F. Borondics,
19
20 *Adv. Sci.*, , DOI:10.1002/advs.201903004.
21
- 22 27 A. H. Colagar, M. J. Chaichi and T. Khadjvand, *J. Biosci.*, 2011, **36**, 669–677.
23
- 24 28 A. M. Banas, K. Banas, T. T. T. Chu, R. Naidu, P. E. Hutchinson, R. Agrawal, M. K. F.
25
26 Lo, M. Kansiz, A. Roy, R. Chandramohanadas and M. B. H. Breese, *Commun. Chem.*,
27
28 2021, **4**, 1–12.
29
- 30 29 D. Etezadi, J. B. Warner, H. A. Lashuel and H. Altug, *ACS Sensors*, 2018, **3**, 1109–1117.
31
- 32 30 E. Benedetti, E. Bramanti, F. Papineschi, I. Rossi and E. Benedetti, *Appl. Spectrosc.*,
33
34 1997, **51**, 792–797.
35
- 36 31 E. Benedetti, P. Vergamini and G. Spremolla, *Mikrochim. Acta*, 1988, **94**, 139–141.
37
- 38 32 W. F. Wolkers and H. Oldenhof, *Spectroscopy*, 2010, **24**, 525–534.
39
- 40 33 K. Hiramatsu, T. Ideguchi, Y. Yonamine, S. Lee, Y. Luo, K. Hashimoto, T. Ito, M. Hase,
41
42 J. Park, Y. Kasai, S. Sakuma, T. Hayakawa, F. Arai, Y. Hoshino and K. Goda, *Sci. Adv.*,
43
44 2019, **5**, eaau0241.
45
46
47
48
49
50
51
52
53
54
55
56
57
58
59
60